

---

---

# Preclinical Evaluation of <sup>111</sup>In-Labeled PEGylated Maytansine Nimotuzumab Drug Conjugates in EGFR-Positive Cancer Models

Siddesh V. Hartimath<sup>1</sup>, Elahe Alizadeh<sup>1</sup>, Viswas Raja Solomon<sup>1</sup>, Rufael Chekol<sup>1</sup>, Wendy Bernhard<sup>2</sup>, Wayne Hill<sup>2</sup>, Angel Casaco Parada<sup>3</sup>, Kris Barreto<sup>2</sup>, Clarence Ronald Geyer<sup>2</sup>, and Humphrey Fonge<sup>1,4</sup>

<sup>1</sup>Department of Medical Imaging, University of Saskatchewan, College of Medicine, Saskatoon SK, Canada; <sup>2</sup>Department of Pathology and Laboratory Medicine, University of Saskatchewan, College of Medicine, Saskatoon SK, Canada; <sup>3</sup>Centre for Molecular Immunology, Havana, Cuba; and <sup>4</sup>Department of Medical Imaging, Royal University Hospital (RUH), Saskatoon SK, Canada

Epidermal growth factor receptor I (EGFR) is overexpressed in most cancers of epithelial origin. Antibody drug conjugates (ADCs) with PEGylated-maytansine (PEG-DM1) show promise in vitro and in vivo. However, in vivo biodistribution data for ADCs with PEG-DM1 have not been reported. Development of methods to understand the real-time in vivo behavior of these ADCs is needed to move these compounds to the clinic. **Methods:** Here we have used noninvasive small-animal SPECT/CT imaging and ex vivo biodistribution to understand the in vivo behavior of PEG<sub>6</sub>-DM1 ADCs. We developed nimotuzumab ADCs conjugated to PEG<sub>6</sub>-DM1. We generated immunoconjugates with low (nimotuzumab-PEG<sub>6</sub>-DM1-Low) and high (nimotuzumab-PEG<sub>6</sub>-DM1-High) drug-to-antibody ratios. The drug-to-antibody of nimotuzumab-PEG<sub>6</sub>-DM1-Low and nimotuzumab-PEG<sub>6</sub>-DM1-High was 3.5 and 7.3, respectively. Quality control was performed using ultraviolet spectrophotometry, size-exclusion high-performance liquid chromatography, bioanalyzer, biolayer interferometry, and flow cytometry in EGFR-positive DLD-1 cells. These immunoconjugates were conjugated with DOTA and radiolabeled with <sup>111</sup>In. The in vitro binding and internalization rates of <sup>111</sup>In-nimotuzumab, <sup>111</sup>In-nimotuzumab-PEG<sub>6</sub>-DM1-Low, and <sup>111</sup>In-nimotuzumab-PEG<sub>6</sub>-DM1-High were characterized. Furthermore, the pharmacokinetics, biodistribution, and imaging characteristics were evaluated in normal and DLD-1 tumor-bearing mice. **Results:** Flow cytometry and biolayer interferometry showed a trend toward decreasing EGFR affinity with increasing number of PEG<sub>6</sub>-DM1 on the antibody. Despite the lower overall cellular binding of the PEG<sub>6</sub>-DM1 radioimmunoconjugates, internalization was higher for PEG<sub>6</sub>-DM1 ADCs than for the non-PEGylated ADC in the following order: <sup>111</sup>In-nimotuzumab-PEG<sub>6</sub>-DM1-High > <sup>111</sup>In-nimotuzumab-PEG<sub>6</sub>-DM1-Low > <sup>111</sup>In-nimotuzumab. Nuclear uptake of <sup>111</sup>In-nimotuzumab-PEG<sub>6</sub>-DM1-High was 4.4-fold higher than <sup>111</sup>In-nimotuzumab. Pharmacokinetics and biodistribution showed that <sup>111</sup>In-nimotuzumab-PEG<sub>6</sub>-DM1-High had the slowest blood and whole-body clearance rate. Uptake in DLD-1 tumors of <sup>111</sup>In-nimotuzumab was similar to <sup>111</sup>In-nimotuzumab-PEG<sub>6</sub>-DM1-Low but was significantly higher than for <sup>111</sup>In-nimotuzumab-PEG<sub>6</sub>-DM1-High. Tumor-to-background ratios for <sup>111</sup>In-nimotuzumab and <sup>111</sup>In-nimotuzumab-PEG<sub>6</sub>-DM1-Low were higher than for <sup>111</sup>In-nimotuzumab-PEG<sub>6</sub>-DM1-High. **Conclusion:** The results show that conjugation of multiple PEG<sub>6</sub>-DM1 reduces the affinity for EGFR in vitro. However,

the reduced affinity is counteracted by the high internalization rate of constructs with PEG<sub>6</sub>-DM1 ADCs in vitro. The decreased affinity resulted in low tumor uptake of <sup>111</sup>In-nimotuzumab-PEG<sub>6</sub>-DM1-High, with a slow overall whole-body clearance rate. These data provide insights for evaluating the pharmacokinetics and normal -tissue toxicity and in determining dosing rate of PEGylated ADCs.

**Key Words:** microSPECT/CT imaging; EGFR; ADCs; nimotuzumab; PEGylated maytansine

**J Nucl Med 2019; 60:1103–1110**  
DOI: 10.2967/jnumed.118.220095

**T**he human epidermal growth factor receptor (EGFR), also known as EGFR/ERBB1/HER1 (human epidermal growth factor receptor 1), is a 170-kDa transmembrane cell surface glycoprotein belonging to the subfamily of type I tyrosine kinase receptor. Other members of this family include ERBB2/HER2, ERBB3/HER3, and ERBB4/HER4 (1). Overexpression of EGFR is implicated in aggressive cancers of epithelial origin, including squamous cell head and neck (90%–100%) (2), glioma (90%–100%) (3), non-small cell lung (75%–90%), colorectal (80%–85%) (4), breast (20%–30%) (5), and cervical (6) cancers. Anti-EGFR antibodies cetuximab (7), panitumumab (8), and nimotuzumab (9,10) are used to treat different EGFR-positive cancers. With the exception of nimotuzumab, these antibodies are associated with significant cutaneous toxicity in 45%–100% of patients (11–13). In contrast, nimotuzumab is better tolerated (10,14) and has low skin toxicities, because its binding affinity is 10-fold lower than other anti-EGFR antibodies, ensuring transient binding to low EGFR-expressing healthy tissues such as the skin (15).

The efficacy of anti-EGFR antibodies is poor (16,17), but efficacy is improved by creating antibody drug conjugates (ADCs) (18). AMG-595 is an anti-EGFR ADC in phase I/II trials in which the antibody is conjugated to a cytotoxic agent maytansine (DM1) (19). Anti-HER2 monoclonal antibody trastuzumab conjugated to DM1 (Kadcyla [Genentech]; trastuzumab-emtansine) is effective in preclinical models and in patients with HER2-positive trastuzumab- or lapatinib-resistant phenotypes and is currently approved (20,21). Despite improvements in efficacy, acquired resistance through the expression of multidrug resistant gene (MDR1) by cancer cells is common with ADCs. Many cytotoxic small molecules including DM1 are substrates for MDR1 and are actively pumped out of the

Received Sep. 5, 2018; revision accepted Dec. 10, 2018.

For correspondence or reprints contact: Humphrey Fonge, Department of Medical Imaging, Room 1566, RUH Saskatoon, 103 Hospital Dr., Saskatoon, SK, S7N 0W8 Canada.

E-mail: humphrey.fonge@usask.ca

Published online Jan. 17, 2019.

COPYRIGHT © 2019 by the Society of Nuclear Medicine and Molecular Imaging.

cell (22–24). ADCs developed with PEGylated DM1 (PEG-DM1), however, are more potent and are not a MDR1 substrate (24,25). These ADCs are also more hydrophilic, allowing conjugation of many drugs without affecting binding to antigens (24,25). These ADCs were severalfold more potent *in vitro* and are effective against resistant cells that overexpress MDR1. Despite these promising *in vitro* results, detailed studies that investigate effects of multiple drugs on antibodies *in vivo* are not available in the literature.

Molecular imaging allows noninvasive *in vivo* assessment of the effects of drugs on the antibody. In the current study, we developed nimotuzumab ADCs using PEG<sub>6</sub>-DM1 with low (nimotuzumab-PEG<sub>6</sub>-DM1-Low) and high (nimotuzumab-PEG<sub>6</sub>-DM1-High) drug-to-antibody ratios (DARs). To understand the effect of multiple drugs conjugated randomly to the antibody, we radiolabeled nimotuzumab-PEG<sub>6</sub>-DM1-Low, nimotuzumab-PEG<sub>6</sub>-DM1-High, and nimotuzumab with <sup>111</sup>In via a DOTA chelator and studied the *in vitro* binding characteristics and *in vivo* behavior using  $\gamma$ -counting techniques and SPECT/CT (small-animal SPECT/CT) imaging. Comparison of the *in vitro* and *in vivo* characteristics of <sup>111</sup>In-nimotuzumab-PEG<sub>6</sub>-DM1-Low, <sup>111</sup>In-nimotuzumab-PEG<sub>6</sub>-DM1-High, and <sup>111</sup>In-nimotuzumab allowed for the real-time assessment of the effects of drugs on the antibody. The development of *in vivo* methods to understand the behavior of ADCs is important because it will enable the quantification of the receptor in real time and the understanding of the complete *in vivo* characteristics of the ADC, which is important in determining treatment regimens and normal-tissue toxicity. If incorporated in clinical trials, this approach could allow for improved dosing regimens and in clinical practice could be used to stratify patients, which can lead to better treatment outcomes using ADCs.

## MATERIALS AND METHODS

DM1 drug was obtained from Toronto Research Chemicals, and NHS-PEG<sub>6</sub>-maleimide was purchased from Biochempeg. DLD-1 (high EGFR density/cell) and HT-29 (low EGFR density/cell) were obtained from American Type Culture Collection and cultured in monolayers in RPMI-1640 and Dulbecco modified Eagle medium/McCoy's 5A media, respectively. All media were supplemented with 10% fetal calf serum, and cells were maintained in a humidified atmosphere with 5% CO<sub>2</sub> at 37°C. Proton MR (<sup>1</sup>HNMR) spectra were obtained on a Bruker NMR, and the exact mass was determined with time-of-flight mass spectrometry (Waters Corp.).

### Synthesis of Nimotuzumab ADCs and Conjugation with p-SCN-Bz-DOTA

Nimotuzumab or control human antibody antimaltose binding protein (MBP IgG) was conjugated with DM1-PEG<sub>6</sub>-NHS. A stock solution (20 mg/mL in dimethyl sulfoxide [DMSO]) of the drug linker DM1-PEG<sub>6</sub>-NHS was prepared. The conjugation reactions were optimized for pH, buffers, and reaction time. To prepare ADCs with a low (3–4) or a high (7–8) DAR, a 5- to 50-mol excess equivalent of drug linker DM1-PEG<sub>6</sub>-NHS was used to conjugate the antibodies to obtain a low (nimotuzumab-PEG<sub>6</sub>-DM1-Low) or high (nimotuzumab-PEG<sub>6</sub>-DM1-High) DAR. Nimotuzumab (5 mg/mL in phosphate-buffered saline [PBS]) was buffer-exchanged using centrifugal filters (Amicon Ultra-4 Centrifugal Filter 10K NMCO; EMD Millipore) and allowed to react with DM1-PEG<sub>6</sub>-NHS for 3–20 h at ambient temperature. In all reactions, the amount of DMSO was kept at less than 3%. The excess unconjugated drug linker was removed from the reaction mixture using a centrifugal filter, and the antibody was stored in PBS. All the conjugates were passed through 0.2- $\mu$ m membrane filters and aliquoted into 20- $\mu$ L vials and stored at –80°C until further use. The DAR was then

determined by ultraviolet spectrophotometry (26) and Bioanalyzer (Agilent).

For DOTA conjugation, a 25-fold excess of p-SCN-Bz-DOTA (20 mg/mL in DMSO) was incubated for 1 h at 37°C with shaking at 500 rpm, with antibodies (5 mg/mL) buffer-exchanged into 0.1 M NaHCO<sub>3</sub> (pH 8.5). Antibodies were stored and excess DOTA removed as described above. Protein concentration was determined by SmartSpec Plus spectrophotometer (Bio-Rad).

### Binding Kinetics and Flow Cytometry

Binding kinetics between antibodies and target proteins were measured using ForteBio Octet RED384 (PALL Corp.). Antibodies were immobilized on antihuman FAB-CH1 sensors (18-5104; Forte Bio) according to the manufacturer's instructions. The equilibrium dissociation constant ( $K_D$ ) was obtained using a 1:1 model with global fitting. Data analysis and curve fitting were performed using data analysis software (version 7.1.0.33; Forte Bio).

DLD-1 or HT-29 cells were treated with antibodies at 10 concentrations starting with 2  $\mu$ M with 3-fold serial dilutions and incubated for 30 min at room temperature followed by 15 min on ice. Cells were washed with PBS + 2% fetal bovine serum and incubated with secondary antibody fluorescein isothiocyanate (FITC)-labeled goat F(ab')<sub>2</sub> fragment antihuman IgG (H + L) (1:50 ratio) (IM0839; Beckman Coulter) for 30 min at 4°C, then washed again. Flow data were acquired using a MACS quant VYB (Miltenyl Biotech) and analyzed by FlowJo (version 10.6; FlowJo LLC). The half maximal effective concentration ( $EC_{50}$ ) was determined using GraphPad Prism 6 (GraphPad Software).

### Radioligand Binding, Internalization, and Immunoreactivity

Binding was determined with DLD-1 cells. A saturation radioligand binding assay was performed by incubating 0.5 million cells with increasing concentrations of radioimmunoconjugates (0.2–95 nmol/L in 100  $\mu$ L of PBS) for 4 h at 4°C. Nonspecific binding was determined in the presence of a 25-fold molar excess of unlabeled nimotuzumab (relative to the highest concentration of the radioimmunoconjugates). A nonlinear regression analysis with 1-site binding equation was used to determine  $K_D$  using GraphPad Prism 6.

Internalization of ADCs is a critical factor that determines efficacy. Internalization of the radioimmunoconjugates was performed using the Nuclei Isolation kit (NUC101; Sigma) as described earlier (27). The immunoreactive fraction of the radioimmunoconjugates was determined as described in Lindmo et al. (28).

### Biodistribution and Pharmacokinetics

Biodistribution was performed in healthy BALB/c mice. Mice ( $n = 4$ /group) were injected with  $6.5 \pm 0.2$  MBq of the radioimmunoconjugates, and animals were sacrificed at 24, 72, or 144 h after injection. Organs were harvested, and activity was measured using a  $\gamma$ -counter (2480; PerkinElmer). Tissue uptake was expressed as percentage injected activity per gram (%IA/g).

The pharmacokinetics were determined in healthy BALB/c mice ( $n = 4$ /group). The animals were injected with  $6.5 \pm 0.1$  MBq of the radioimmunoconjugates via a tail vein, and blood was collected at various time points from a saphenous vein in heparinized capillary tubes. Radioactivity in blood activity was expressed as %IA per milliliter. Relevant pharmacokinetic parameters were determined using an exponential decay curve fitting from  $\sigma$ -plot using GraphPad Prism 6.

### Small-Animal SPECT/CT Imaging

DLD-1 tumor-bearing mice were injected via a tail vein with 12–15 MBq of radioimmunoconjugates. The mice were anesthetized using isoflurane/oxygen (5% induction and 2% maintenance), and SPECT/CT images were acquired at 24, 48, 72, 96, 120, 144, and 168 h after injection using the Vector<sup>4</sup>CT scanner (MILabs B.V.). A 30-min full body SPECT scan was acquired in a list-mode data format with a

TABLE 1

Equilibrium Dissociation Constant ( $K_D$ ), Association Constants ( $K_{on}$ ), and Dissociation Constants ( $K_{diss}$ ), by Biolayer Interferometry of Antibody and Immunoconjugates

Construct	$K_D$ (nM)	$K_{on}$ (1/Ms)	$K_{diss}$ (1/s)
Nimotuzumab	$0.62 \pm 0.01$	$5.8 \pm 0.02 \times 10^4$	$3.2 \pm 0.06 \times 10^{-5}$
DOTA-nimotuzumab	$1.05 \pm 0.13$	$7.38 \pm 0.02 \times 10^4$	$7.76 \pm 0.05 \times 10^{-5}$
DOTA-nimotuzumab-PEG <sub>6</sub> -DM1-Low	$3.53 \pm 0.04$	$6.25 \pm 0.03 \times 10^4$	$1.95 \pm 0.02 \times 10^{-4}$
DOTA-nimotuzumab-PEG <sub>6</sub> -DM1-High	$13.02 \pm 0.01$	$3.77 \pm 0.09 \times 10^4$	$4.91 \pm 0.03 \times 10^{-4}$

high-energy ultra-high-resolution mouse pinhole collimator (HE-UHR-1.0 mm) followed by full-body CT scan with a tube setting of 50 kV and 480  $\mu$ A. The body temperature, heart rate, and respiration of animals were continuously monitored.

Images were reconstructed with a pixel-based ordered-subset expectation maximization algorithm that included resolution recovery and compensation for distance-dependent pinhole sensitivity. For the SPECT images, we used 16 subsets and 10 iterations (160 ML-EM equivalent) image reconstruction with an isotropic 0.8-mm voxel grid. CT images were reconstructed using Hann projection with a filter of a 150-mm voxel grid to generate a 3-dimensional CT image. Reconstructed SPECT images were quantified to correct for attenuation, using the CT image as an attenuation map for nonuniform attenuation correction. The registered CT and quantified SPECT images were analyzed using PMOD software (version 3.8; PMOD Technologies). A region of interest was manually drawn around the tumor, heart, liver, muscle, kidneys, and bladder, and uptake was expressed as mean percentage injected activity per volume (%IA/cc  $\pm$  SD). At the end of imaging (168 h after injection), mice were euthanized, followed by biodistribution studies. Uptake in all organs was expressed as %IA/g

#### Statistical Analysis

All data were expressed as the mean  $\pm$  SD or SEM of at least 3 independent experiments. Statistical significance between groups was assessed using a 2-tailed Student *t*-test or ANOVA with Bonferroni post hoc test. Graphs were prepared and analyzed using GraphPad Prism (version 6; GraphPad Software).

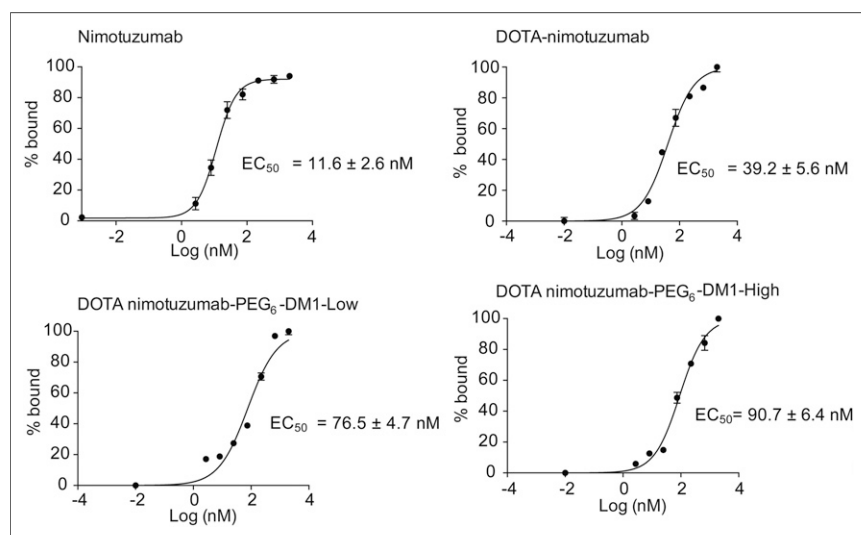


**FIGURE 1.** In vitro flow cytometry binding assay. DLD-1 cells were titrated with nimotuzumab, DOTA-nimotuzumab, DOTA-nimotuzumab-PEG<sub>6</sub>-DM1-Low, and DOTA-nimotuzumab-PEG<sub>6</sub>-DM1-High and analyzed by flow cytometry.

## RESULTS

### Characterization of Immunoconjugates

We developed nimotuzumab ADCs nimotuzumab-PEG<sub>6</sub>-DM1-Low and nimotuzumab-PEG<sub>6</sub>-DM1-High with low ( $\sim$ 3.5) and high ( $\sim$ 7.3) DARs (Supplemental Figs. 1 and 2; supplemental materials are available at <http://jnm.snmjournals.org>). Nimotuzumab, nimotuzumab-PEG<sub>6</sub>-DM1-Low, and nimotuzumab-PEG<sub>6</sub>-DM1-High were conjugated to DOTA to allow radiolabeling with <sup>111</sup>In (Supplemental Fig. 3). High-performance liquid chromatography showed that the conjugates were greater than 98% pure with less than 1% aggregates or degradation (Supplemental Fig. 4). Bioanalyzer showed the purity and size of nimotuzumab, nimotuzumab-PEG<sub>6</sub>-DM1-Low, nimotuzumab-PEG<sub>6</sub>-DM1-High, and their respective DOTA-conjugated immunoconjugates (Supplemental Fig. 5A)

The effect of DOTA conjugation on the  $K_D$  to recombinant EGFR was studied using biolayer interferometry (Supplemental Fig. 5B; Table 1). The  $K_D$  of DOTA-nimotuzumab was not significantly different ( $P = 0.09$ ) from nimotuzumab. However, the  $K_D$ s of DOTA-nimotuzumab-PEG<sub>6</sub>-DM1-Low and DOTA-nimotuzumab-PEG<sub>6</sub>-DM1-High were, respectively, 5.7-fold ( $P < 0.05$ ) and 21-fold ( $P = 0.05$ ) higher than for nimotuzumab (Table 1).

The binding of the immunoconjugates to EGFR-positive DLD-1 (high EGFR expression) and HT-29 (low EGFR expression) cells was studied by flow cytometry (Fig. 1). The EC<sub>50</sub> of nimotuzumab was 3.4-fold lower than DOTA-nimotuzumab ( $11.6 \pm 2.6$  nM vs.  $39.2 \pm 5.6$  nM;  $P = 0.79$ ). The EC<sub>50</sub> of DOTA-nimotuzumab-PEG<sub>6</sub>-DM1-Low ( $76.5 \pm 4.8$  nM) and DOTA-nimotuzumab-PEG<sub>6</sub>-DM1-High ( $90.7 \pm 6.4$  nM) was, respectively, 2-fold ( $P < 0.05$ ) and 2.3-fold ( $P < 0.05$ ) higher than DOTA-nimotuzumab.

### Radiolabeling and Stability of Radioimmunoconjugates

To optimize the labeling with <sup>111</sup>In, different radiolabeling conditions were studied: time (60 or 90 min), temperature (room temperature or 37°C), pH (4.5–6), and specific activity (0.1–1.5 MBq/ $\mu$ g). The best radiochemical yield was obtained using 0.5 MBq/ $\mu$ g, pH 5.0, at room temperature after 90-min incubation. Under these conditions, the average radiochemical yield for all the tracers was  $65\% \pm 3\%$ , with a radiochemical purity of greater than 98% (Supplemental Fig. 4).

The radioimmunoconjugates were stable in human plasma and PBS after incubation at 37°C for 5 d (Supplemental Fig. 6A).

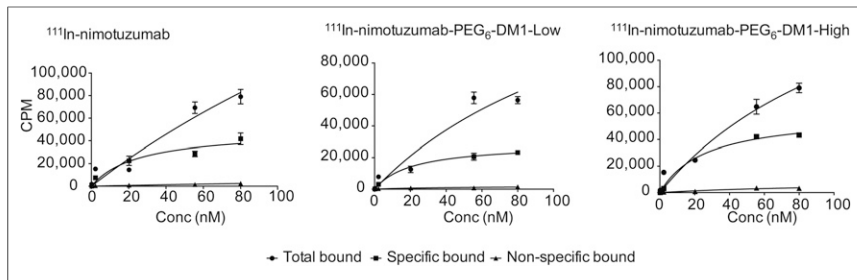


**FIGURE 2.** Saturation radioligand binding assay.  $^{111}\text{In}$ -nimotuzumab,  $^{111}\text{In}$ -nimotuzumab-PEG<sub>6</sub>-DM1-Low, and  $^{111}\text{In}$ -nimotuzumab-PEG<sub>6</sub>-DM1-High were tested for binding to EGFR-positive DLD-1 cells. Conc = concentration; CPM = counts per minute.

Dissociation of  $^{111}\text{In}$  from the complex was studied in challenge experiments using a severalfold excess of other metal ions:  $\text{Ca}^{2+}$ ,  $\text{Mg}^{2+}$ ,  $\text{Fe}^{2+}$ , and  $\text{Zn}^{2+}$ . All radioimmunoconjugates showed dissociation in the presence of 1 M  $\text{Fe}^{2+}$  ions, with 50% released from the DOTA complex (Supplemental Figs. 6B–6D).

### Radioligand Binding and Immunoreactivity

To verify whether radiolabeling affected the binding of the radioimmunoconjugates, a saturation binding assay was performed using EGFR-positive DLD-1 cells (Fig. 2). The estimated  $K_D$  of  $^{111}\text{In}$ -nimotuzumab,  $^{111}\text{In}$ -nimotuzumab-PEG<sub>6</sub>-DM1-Low, and  $^{111}\text{In}$ -nimotuzumab-PEG<sub>6</sub>-DM1-High was  $25 \pm 4.3$ ,  $167 \pm 6.3$ , and  $303 \pm 8.6$  nM, respectively. The values for  $^{111}\text{In}$ -nimotuzumab-PEG<sub>6</sub>-DM1-Low and  $^{111}\text{In}$ -nimotuzumab-PEG<sub>6</sub>-DM1-

High were, respectively, 6-fold ( $P < 0.05$ ) and 12-fold ( $P < 0.05$ ) higher than for  $^{111}\text{In}$ -nimotuzumab.

The immunoreactive fraction of  $^{111}\text{In}$ -nimotuzumab,  $^{111}\text{In}$ -nimotuzumab-PEG<sub>6</sub>-DM1-Low, and  $^{111}\text{In}$ -nimotuzumab-PEG<sub>6</sub>-DM1-High was 0.83, 0.70, and 0.58, respectively (Supplemental Fig. 7). There was a decrease in the immunoreactive fraction of the antibody with increasing number of drugs on the antibody. The immunoreactive fraction of  $^{111}\text{In}$ -nimotuzumab-PEG<sub>6</sub>-DM1-High was significantly lower ( $P < 0.05$ ) than  $^{111}\text{In}$ -nimotuzumab.

### Internalization of Radioimmunoconjugates

Internalization of all radioimmunoconjugates increased over time (Fig. 3A). The highest internalization rate was observed at 48 h after incubation with  $^{111}\text{In}$ -nimotuzumab-PEG<sub>6</sub>-DM1-High (41%) >  $^{111}\text{In}$ -nimotuzumab-PEG<sub>6</sub>-DM1-Low (40%) >  $^{111}\text{In}$ -nimotuzumab (37%). The amount of membrane-bound immunoconjugate was highest for  $^{111}\text{In}$ -nimotuzumab followed by  $^{111}\text{In}$ -nimotuzumab-PEG<sub>6</sub>-DM1-Low and  $^{111}\text{In}$ -nimotuzumab-PEG<sub>6</sub>-DM1-high (Fig. 3B), which was in line with the lowest  $K_D$  for  $^{111}\text{In}$ -nimotuzumab. Cytoplasmic-bound tracer increased in the order  $^{111}\text{In}$ -nimotuzumab >  $^{111}\text{In}$ -nimotuzumab-PEG<sub>6</sub>-DM1-Low >  $^{111}\text{In}$ -nimotuzumab-PEG<sub>6</sub>-DM1-High (Fig. 3C), with a statistically higher ( $P < 0.05$ ) cytoplasmic uptake of  $^{111}\text{In}$ -nimotuzumab than  $^{111}\text{In}$ -nimotuzumab-PEG<sub>6</sub>-DM1-Low and  $^{111}\text{In}$ -nimotuzumab-PEG<sub>6</sub>-DM1-High. Interestingly, the nuclear-bound fraction was similar for  $^{111}\text{In}$ -nimotuzumab-PEG<sub>6</sub>-DM1-Low and  $^{111}\text{In}$ -nimotuzumab-PEG<sub>6</sub>-DM1-High and was significantly ( $P < 0.05$ ) higher than  $^{111}\text{In}$ -nimotuzumab (Fig. 3D). The highest nuclear uptake was observed at 4 h for the drug conjugates ( $^{111}\text{In}$ -nimotuzumab-PEG<sub>6</sub>-DM1-Low [48.4%] vs.  $^{111}\text{In}$ -nimotuzumab-PEG<sub>6</sub>-DM1-High [53.1%]) and decreased thereafter. There was negligible uptake of the control antibody  $^{111}\text{In}$ -ctrl-IgG and drug conjugates of the control antibody  $^{111}\text{In}$ -ctrl-IgG-PEG<sub>6</sub>-DM1-Low and  $^{111}\text{In}$ -ctrl-IgG-PEG<sub>6</sub>-DM1-High (Fig. 3A).

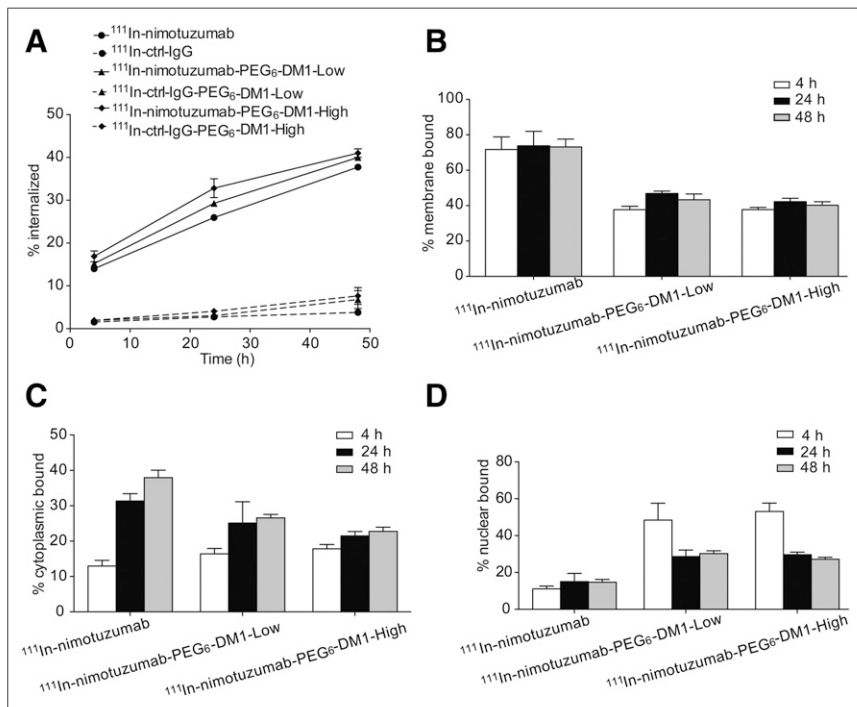


**FIGURE 3.** EGFR-mediated internalization. (A)  $^{111}\text{In}$ -nimotuzumab,  $^{111}\text{In}$ -nimotuzumab-PEG<sub>6</sub>-DM1-Low,  $^{111}\text{In}$ -nimotuzumab-PEG<sub>6</sub>-DM1-High, control antibody ( $^{111}\text{In}$ -ctrl-IgG), and control ADCs ( $^{111}\text{In}$ -ctrl-IgG-PEG<sub>6</sub>-DM1-Low and  $^{111}\text{In}$ -ctrl-IgG-PEG<sub>6</sub>-DM1-High) were tested for EGFR-mediated internalization using DLD-1 cells at 4, 24, and 48 h (h) after incubation. (A) Total internalized radioimmunoconjugate. (B) Total membrane bound. (C) Cytoplasmic bound. (D) Nuclear uptake.

### Biodistribution and Pharmacokinetics

Normal-tissue biodistribution of  $^{111}\text{In}$ -nimotuzumab,  $^{111}\text{In}$ -nimotuzumab-PEG<sub>6</sub>-DM1-Low, and  $^{111}\text{In}$ -nimotuzumab-PEG<sub>6</sub>-DM1-High was studied in healthy BALB/c mice ( $n = 4$ /tracer and time point) at 24, 72, and 144 h after injection (Figs. 4A–4C). Whole-body clearance of the tracer was slowest for  $^{111}\text{In}$ -nimotuzumab-PEG<sub>6</sub>-DM1-High. Clearance from major organs was in the order  $^{111}\text{In}$ -nimotuzumab-PEG<sub>6</sub>-DM1-High <  $^{111}\text{In}$ -nimotuzumab-PEG<sub>6</sub>-DM1-Low <  $^{111}\text{In}$ -nimotuzumab. The clearance was largely determined by the half-life in blood, with  $^{111}\text{In}$ -nimotuzumab-PEG<sub>6</sub>-DM1-High showing the highest blood retention at

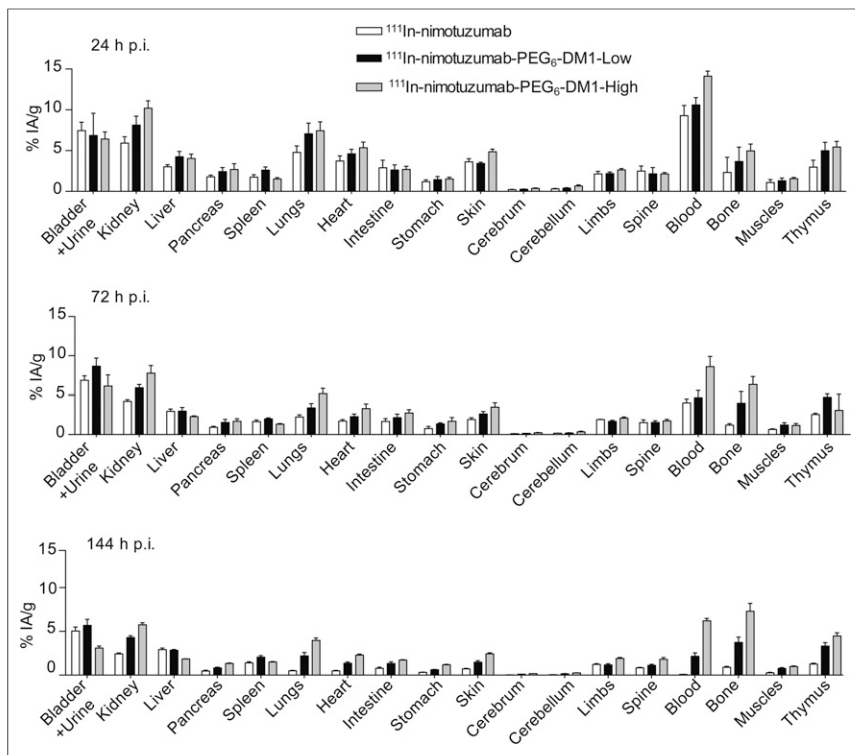


**FIGURE 4.** Biodistribution in healthy BALB/c mice of  $^{111}\text{In}$ -nimotuzumab,  $^{111}\text{In}$ -nimotuzumab-PEG<sub>6</sub>-DM1-Low, and  $^{111}\text{In}$ -nimotuzumab-PEG<sub>6</sub>-DM1-High at 24, 72, and 144 h after injection (p.i.).

all time points. At 144 h after injection,  $^{111}\text{In}$ -nimotuzumab was almost completely cleared from all organs except for the liver ( $2.91 \pm 0.37$  %IA/g) and kidney ( $2.41 \pm 0.23$  %IA/g). There was a higher residual bone uptake of the  $^{111}\text{In}$ -nimotuzumab-PEG<sub>6</sub>-DM1-High and  $^{111}\text{In}$ -nimotuzumab-PEG<sub>6</sub>-DM1-Low than of  $^{111}\text{In}$ -nimotuzumab, with the highest uptake observed at 144 h. The presence of the PEG<sub>6</sub>-DM1 led to significantly higher renal clearance of the  $^{111}\text{In}$ -nimotuzumab-PEG<sub>6</sub>-DM1-Low and  $^{111}\text{In}$ -nimotuzumab-PEG<sub>6</sub>-DM1-High than the  $^{111}\text{In}$ -nimotuzumab immunoconjugate.

The pharmacokinetics of all radioimmunoconjugates were studied in normal BALB/c mice (Fig. 5). All tracers exhibited a biphasic half-life with a fast (distribution)  $t_{1/2\alpha}$  and a slow clearance  $t_{1/2\beta}$  (Table 2). There was a trend toward longer circulation with the number of drugs (PEG<sub>6</sub>-DM1) on the antibody, with the  $^{111}\text{In}$ -nimotuzumab-PEG<sub>6</sub>-DM1-High exhibiting the longest circulation time, with the exception of area under the curve (AUC), which was longest ( $P < 0.05$ ) for  $^{111}\text{In}$ -nimotuzumab-PEG<sub>6</sub>-DM1-High. No significant differences were found for all of the pharmacokinetic parameters studied.

#### Small-Animal SPECT Imaging and Biodistribution in Mouse Xenograft

Small-animal SPECT imaging was performed in athymic CD-1 nude mice bearing DLD-1 xenografts at different time points (Fig. 6A). Unequivocal delineation of xenograft was seen with nimotuzumab radioimmunoconjugates at 48 h after injection and remained persistent at 168 h after injection.  $^{111}\text{In}$ -ctrl-IgG had negligible tumor uptake. As with all immunoglobulins, intense liver uptake was visible. Apart from tumor and liver, we also noticed high accumulation in auxiliary lymph nodes in all the groups. Kidneys and bladder were also visible even at 24 h after injection but decreased at later time points.

Time-activity curves were generated for tumor (Fig. 6B). No significant difference in tumor uptake was seen between  $^{111}\text{In}$ -nimotuzumab and  $^{111}\text{In}$ -nimotuzumab-PEG<sub>6</sub>-DM1-Low at any time point. However, tumor uptake was significantly higher for  $^{111}\text{In}$ -nimotuzumab than  $^{111}\text{In}$ -nimotuzumab-PEG<sub>6</sub>-DM1-High at later time points (144 h:  $P < 0.0001$ ; and 168 h:  $P < 0.001$ ). Tumor uptake of  $^{111}\text{In}$ -nimotuzumab-PEG<sub>6</sub>-DM1-Low was also higher (48 h:  $P < 0.001$ ; 72 h:  $P < 0.001$ ; 144 h:  $P < 0.0001$ ; and 168 h:  $P < 0.01$ ) than  $^{111}\text{In}$ -nimotuzumab-PEG<sub>6</sub>-DM1-High at all time points except at 24 h ( $P > 0.05$ ) when this difference was not statistically significant. Peak tumor uptake on small-animal SPECT was observed at 72 h and was  $11.8 \pm 0.22$  % IA/cc,  $12.63 \pm 1.08$  %IA/cc, and  $9.83 \pm 1.13$  %IA/cc for  $^{111}\text{In}$ -nimotuzumab,  $^{111}\text{In}$ -nimotuzumab-PEG<sub>6</sub>-DM1-Low, and  $^{111}\text{In}$ -nimotuzumab-PEG<sub>6</sub>-DM1-High, respectively.

There were no differences in liver uptake of  $^{111}\text{In}$ -nimotuzumab compared with  $^{111}\text{In}$ -nimotuzumab-PEG<sub>6</sub>-DM1-Low (Fig. 6C). However, liver uptake of  $^{111}\text{In}$ -nimotuzumab-PEG<sub>6</sub>-DM1-High was slightly higher than  $^{111}\text{In}$ -nimotuzumab and  $^{111}\text{In}$ -nimotuzumab-PEG<sub>6</sub>-DM1-Low; this difference was significant only at later time points. Differences in tumor-to-liver ratios were mostly not statistically significant (Supplemental Fig. 8). On the other hand, tumor-to-muscle ratios were higher for  $^{111}\text{In}$ -nimotuzumab and  $^{111}\text{In}$ -nimotuzumab-PEG<sub>6</sub>-DM1-Low than  $^{111}\text{In}$ -nimotuzumab-PEG<sub>6</sub>-DM1-High at 72, 144, and 168 h time points (Supplemental Fig. 8). Biodistribution at 168 h after injection confirmed the small-animal SPECT observations (Fig. 7). Higher

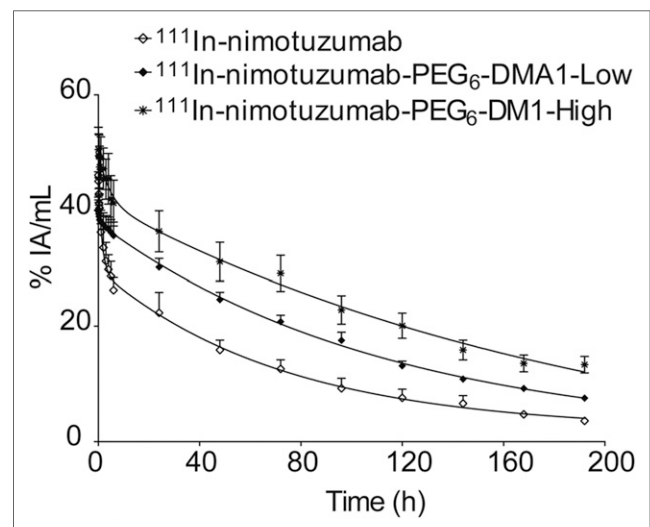


**FIGURE 5.** Pharmacokinetics of  $^{111}\text{In}$ -nimotuzumab,  $^{111}\text{In}$ -nimotuzumab-PEG<sub>6</sub>-DMA1-Low, and  $^{111}\text{In}$ -nimotuzumab-PEG<sub>6</sub>-DM1-High in healthy BALB/c mice.

**TABLE 2**

Pharmacokinetic Parameters of <sup>111</sup>In-Nimotuzumab, <sup>111</sup>In-Nimotuzumab-PEG<sub>6</sub>-DM1-Low, and <sup>111</sup>In-Nimotuzumab-PEG<sub>6</sub>-DM1-High in Healthy BALB/c Mice

Construct	Half-life $t_{1/2\alpha}$ (h)	Half-life $t_{1/2\beta}$ (h)	AUC (%IA h/mL)	$V_{ss}$ (mL)	CL (mL/h $\times 10^{-2}$ )
<sup>111</sup> In-nimotuzumab	2.3 $\pm$ 0.7	165 $\pm$ 29.6	1096.8 $\pm$ 6.3	19.3 $\pm$ 3.9	9.1 $\pm$ 1.0
<sup>111</sup> In-nimotuzumab-PEG <sub>6</sub> -DM1-Low	17.6 $\pm$ 7.3	217.2 $\pm$ 24.7	2293.5 $\pm$ 299.9	10.9 $\pm$ 4.6	5.0 $\pm$ 1.0
<sup>111</sup> In-nimotuzumab-PEG <sub>6</sub> -DM1-High	4.8 $\pm$ 0.1	433.1 $\pm$ 0.0	2791.6 $\pm$ 140.8	19.9 $\pm$ 1.0	4.0 $\pm$ 0.2

Data are mean values  $\pm$  SEM.

$V_{ss}$  = volume of distribution at steady state; CL = clearance rate.

spleen and liver uptake was seen with <sup>111</sup>In-nimotuzumab-PEG<sub>6</sub>-DM1-High.

**DISCUSSION**

Several factors account for why antibodies have not lived up to expectations as immunotherapeutics. De novo and acquired

resistance to immunotherapeutics is a common phenomenon in oncology. Cancer cells develop intrinsic resistance by overexpression of alternate growth factors and their receptors. EGFR overexpression, for example, is a widely accepted mechanism of acquired resistance to HER2-targeted treatments (29). Overexpression of MDR1 is a widely accepted mechanism of de novo resistance by cancer cells to small molecule drugs (22–24). DM1 has been one of the drugs of choice for many ADCs. Once internalized the DM1 is cleaved from the antibody in lysosomes and becomes toxic to the cell. However, there is strong evidence that DM1, just like many other small-molecule therapeutics, is a substrate for MDR1. This effect has been seen with HER2-targeted Kadcyyla (trastuzumab-DM1) as well as AMG-595 (anti-EGFR-DM1) (22,23). However, PEG<sub>6</sub>-DM1, as proposed in this study, is not a substrate of MDR1 (24,25).

An optimum DAR is needed to preserve biologic characteristics of the antibody. Zhao et al. showed that a DAR of 9 using PEG linkers yielded ADCs that were more cytotoxic in vitro than the routinely used DAR of 3–4 (25). In this study, we developed nimotuzumab-PEG<sub>6</sub>-DM1-Low and nimotuzumab-PEG<sub>6</sub>-DM1-High ADCs with DARs of 3.5 and 7.3, respectively. We used in vitro assays, noninvasive real-time small-animal SPECT/CT imaging and ex vivo biodistribution to characterize the behavior of PEGylated nimotuzumab ADC immunoconjugates by radiolabeling the nimotuzumab-PEG<sub>6</sub>-DM1-Low/High with <sup>111</sup>In.

We showed by biolayer interferometry that in comparison with nimotuzumab, the binding of nimotuzumab-PEG<sub>6</sub>-DM1-Low (1.94 nM) and nimotuzumab-PEG<sub>6</sub>-DM1-High (3.75 nM) to recombinant EGFR was lower. The chelator-to-antibody ratio after the conjugation of DOTA was 2.8  $\pm$  0.2 for nimotuzumab, nimotuzumab-PEG<sub>6</sub>-DM1-Low, and nimotuzumab-PEG<sub>6</sub>-DM1-High. Size-exclusion chromatography and bioanalyzer showed that DOTA-nimotuzumab, DOTA-nimotuzumab-PEG<sub>6</sub>-DM1-Low, and

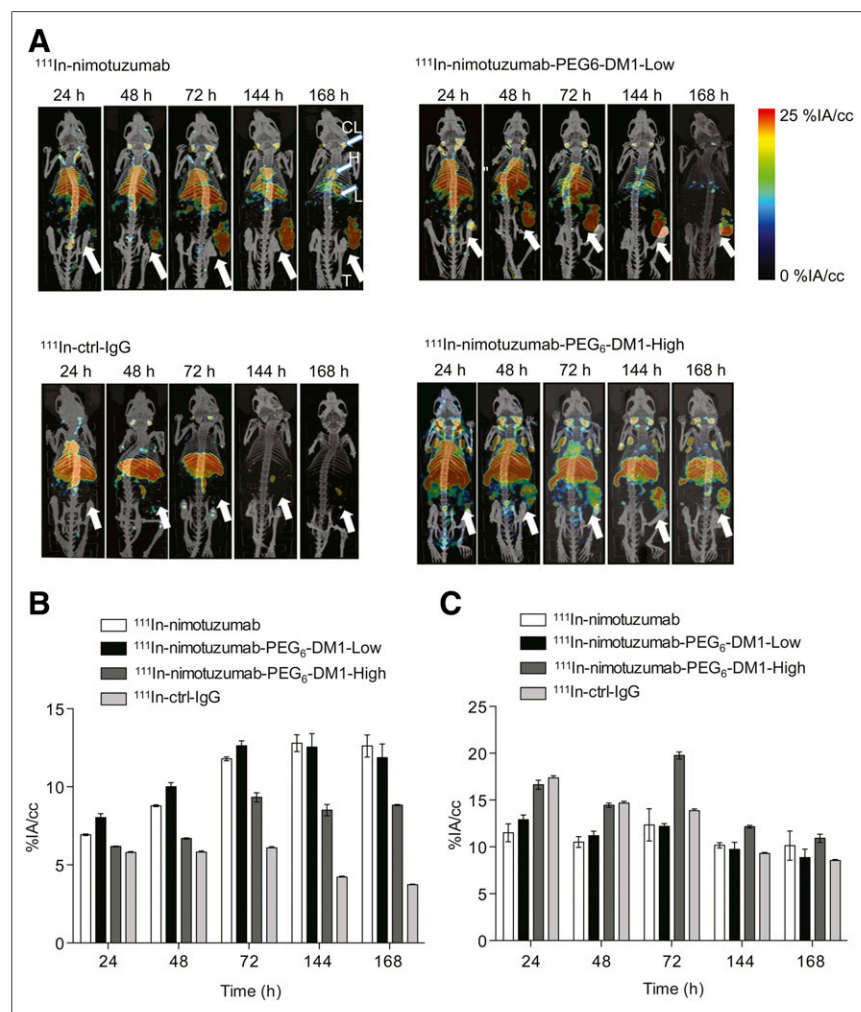


**FIGURE 6.** (A) Small-animal SPECT/CT imaging. <sup>111</sup>In-nimotuzumab, <sup>111</sup>In-nimotuzumab-PEG<sub>6</sub>-DM1-Low, <sup>111</sup>In-nimotuzumab-PEG<sub>6</sub>-DM1-High, and control antibody <sup>111</sup>In-ctrl-IgG small-animal SPECT/CT imaging in mice bearing DLD-1 tumors in their right hind leg (white arrow) at 24, 48, 144, and 168 h after injection ( $n = 4$  per tracer per time point). CL = cervical lymph node; H = heart; L = liver; T = tumor. (B) Tumor time-activity uptake from small-animal SPECT. (C) Liver time-activity uptake.

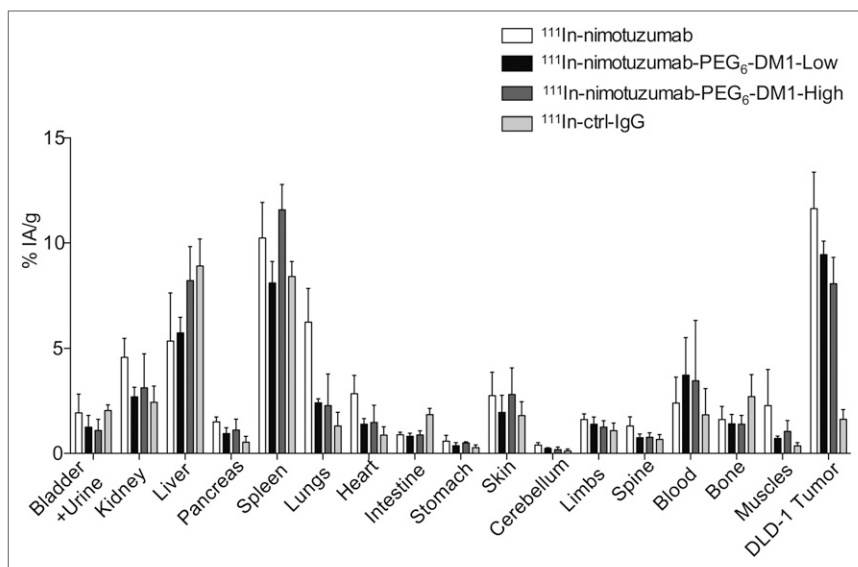


**FIGURE 7.** Biodistribution of  $^{111}\text{In}$ -nimotuzumab,  $^{111}\text{In}$ -nimotuzumab-PEG<sub>6</sub>-DM1-Low,  $^{111}\text{In}$ -nimotuzumab-PEG<sub>6</sub>-DM1-High, and control antibody  $^{111}\text{In}$ -ctrl-IgG in athymic CD-1 nude mice bearing DLD-1 tumors at 168 h after injection.

DOTA-nimotuzumab-PEG<sub>6</sub>-DM1-High were exclusively monomeric species. Conjugation of DOTA led to an increase in  $K_D$  compared with the antibody without DOTA chelator. Flow cytometry showed that binding to cells was altered by conjugation reactions. Saturated radioligand binding experiments show that radiolabeling did not alter the binding of the radioimmunoconjugates to EGFR-positive cells.

The potency of ADCs is dependent on lysosomal processing and release of cleaved lysine-SMCC-DM1, which is then toxic to cancer cells (30). Kovtun et al. showed that PEG<sub>4</sub>-Mal-DM1 conjugated to an anti-EpCAM antibody followed the same lysosomal proteolytic pathway as DM1-conjugated ADCs. Anti-EpCAM-PEG<sub>4</sub>-DM1 was processed by EpCAM-positive cells, resulting in a polar lysine-PEG<sub>4</sub>-DM1 metabolite, which was equally cytotoxic to cells (24). The higher internalization rate of  $^{111}\text{In}$ -nimotuzumab-PEG<sub>6</sub>-DM1-High probably explains the higher in vitro potency of PEG-DM1 immunoconjugates with high DAR. EGFR is a highly internalizing antigen, and it has been shown that binding of anti-EGFR antibodies to EGFR enhances internalization of the antigen-antibody complex (31). Whether the ADCs internalize better than the antibody is very much a matter of debate and depends on the antibody-antigen complex as well as other adapter molecules. Some authors have shown internalization rate for ADCs to be higher than the unconjugated antibody whereas others have shown the opposite or similar rates of internalization (32). Smith et al. (33) showed that antimelanotransferrin ADC in which the antibody (L49) was conjugated to auristatin cytotoxin internalized better than the unconjugated antibody. Similarly, Law et al. (34) compared the rates of internalization of anti-CD20 rituximab, rituximab conjugated to monomethyl auristatin E (rituximab-vcMMAE), or doxorubicin (rituximab-vcDox) in CD20-positive cells. The rate of internalization was highest for rituximab-vcDox followed by rituximab-vcMMAE. Unconjugated rituximab had very low internalization rate in these CD20-positive cells. As was shown for cetuximab-EGFR complex (35), it is possible that the binding of nimotuzumab ADCs follows a similar clathrin-independent (macropinocytosis) pathway, resulting in higher internalization rates and, hence, enhanced processing of the ADCs.

Overall total binding decreased with increasing number of PEG<sub>6</sub>-DM1 on antibody. This was consistent with the higher  $K_D$  of immunoconjugates with drug relative to immunoconjugates alone. Despite lower overall cellular binding, internalization increased with increasing number of drugs on the antibody. Particularly, at 4 h after treatment nuclei uptake of  $^{111}\text{In}$ -nimotuzumab-PEG<sub>6</sub>-DM1-High was similar to  $^{111}\text{In}$ -nimotuzumab-PEG<sub>6</sub>-DM1-Low but was 4.4-fold higher than for  $^{111}\text{In}$ -nimotuzumab. Higher nuclear uptake leads to increased chance of double DNA strand break and hence apoptotic cell death.

Pharmacokinetics and biodistribution in normal mice showed a longer distribution half-life with increasing number of PEG<sub>6</sub>-DM1 on the antibody, with  $^{111}\text{In}$ -nimotuzumab-PEG<sub>6</sub>-DM1-High showing the longest  $t_{1/2\beta}$ . These results correlate with previous studies that showed that PEGylation increases the half-life of peptides and macromolecules (36). Other studies have shown that the higher the number of drugs

(non-PEGylated) on the antibody the faster the clearance of the immunoconjugate from circulation (37,38). The long plasma half-life of  $^{111}\text{In}$ -nimotuzumab-PEG<sub>6</sub>-DM1-High resulted in slow overall clearance of the immunoconjugate from most major organs at 168 h after injection whereas  $^{111}\text{In}$ -nimotuzumab was completely cleared at this time. This longer half-life has implications for dosing of the PEGylated ADCs. Biodistribution in mice bearing DLD-1 xenograft showed a trend toward decreasing tumor uptake with the number of PEG<sub>6</sub>-DM1 on the antibody. Tumor uptake of  $^{111}\text{In}$ -nimotuzumab was similar to  $^{111}\text{In}$ -nimotuzumab-PEG<sub>6</sub>-DM1-Low. However, tumor uptake of  $^{111}\text{In}$ -nimotuzumab was higher than  $^{111}\text{In}$ -nimotuzumab-PEG<sub>6</sub>-DM1-High, implying that the lower EGFR binding of  $^{111}\text{In}$ -nimotuzumab-PEG<sub>6</sub>-DM1-High as evident by the higher  $K_D$  resulted in decreased EGFR binding/uptake in the DLD-1 xenograft in vivo. Small-animal SPECT imaging further confirmed the significantly lower tumor uptake of  $^{111}\text{In}$ -nimotuzumab-PEG<sub>6</sub>-DM1-High at 48, 72, 144, and 168 h after injection. Tumor-to-muscle ratios of  $^{111}\text{In}$ -nimotuzumab-PEG<sub>6</sub>-DM1-High were equally lower than for  $^{111}\text{In}$ -nimotuzumab and  $^{111}\text{In}$ -nimotuzumab-PEG<sub>6</sub>-DM1-Low at most time points.

In this work the ADCs have been radiolabeled at one or more of the lysine residues on the antibody. Although this approach has tremendous potential in the understanding of the in vivo behavior of the ADCs, it does not provide sufficient insights on the rate of lysosomal cleavage/processing of the drug (PEG<sub>6</sub>-DM1) from the antibody, which is partly responsible for the efficacy of the ADC.

## CONCLUSION

In this work, using PEG<sub>6</sub>-DM1, we developed nimotuzumab ADCs with low (nimotuzumab-PEG<sub>6</sub>-DM1-Low: DAR, 3.5) and high (nimotuzumab-PEG<sub>6</sub>-DM1-High: DAR, 7.3) DAR.  $^{111}\text{In}$ -nimotuzumab,  $^{111}\text{In}$ -nimotuzumab-PEG<sub>6</sub>-DM1-Low, and  $^{111}\text{In}$ -nimotuzumab-PEG<sub>6</sub>-DM1-High were developed to understand the effect of drug conjugation on the antibody using small-animal SPECT and ex vivo biodistribution. In vitro characterization of



immunoconjugates showed significantly decreased affinity for EGFR with increasing number of PEG<sub>6</sub>-DM1 on the antibody. Interestingly, ADCs with higher DAR had higher internalization rates, which may account for the higher potency seen with these ADCs. Although there was no differences in tumor uptake between <sup>111</sup>In-nimotuzumab and <sup>111</sup>In-nimotuzumab-PEG<sub>6</sub>-DM1-Low, tumor uptake was significantly lower for <sup>111</sup>In-nimotuzumab-PEG<sub>6</sub>-DM1-High. This result implies that at the same dosing rate nimotuzumab-PEG<sub>6</sub>-DM1-High could be less effective in vivo. This imaging data confirms our recent findings that nimotuzumab-PEG<sub>6</sub>-DM1-Low was more potent than nimotuzumab-PEG<sub>6</sub>-DM1-High in DLD-1 tumors. Administration of 15 mg of nimotuzumab-PEG<sub>6</sub>-DM1-Low per kilogram led to complete remission in 4 of 6 mice whereas same dose resulted in remission in 2 of 6 mice in nimotuzumab-PEG<sub>6</sub>-DM1-High (39). Noninvasive small-animal SPECT imaging allowed for the understanding of the in vivo behavior of the ADCs and can be used to determine dosing.

## DISCLOSURE

This study was funded by a grants from the Canadian Breast Cancer Research (no. 300030) and Saskatchewan Health Research Foundation (no. 3554). Nimotuzumab was provided by the Center for Molecular Immunology (Havana, Cuba) under the terms of a research collaboration agreement. No other potential conflict of interest relevant to this article was reported.

## ACKNOWLEDGMENTS

We acknowledge the contributions of all other members of the Geyer and Fonge Labs. All applicable international, national, or institutional guidelines for the care and use of animals were followed – University of Saskatchewan animal protocol # 20170084.

## REFERENCES

- Robinson DR, Wu YM, Lin SF. The protein tyrosine kinase family of the human genome. *Oncogene*. 2000;19:5548–5557.
- Chung CH, Ely K, McGavran L, et al. Increased epidermal growth factor receptor gene copy number is associated with poor prognosis in head and neck squamous cell carcinomas. *J Clin Oncol*. 2006;24:4170–4176.
- Alshenawy HA. Immunohistochemical expression of epidermal growth factor receptor, E-cadherin, and matrix metalloproteinase-9 in ovarian epithelial cancer and relation to patient deaths. *Ann Diagn Pathol*. 2010;14:387–395.
- Cunningham D, Humblet Y, Siena S, et al. Cetuximab monotherapy and cetuximab plus irinotecan in irinotecan-refractory metastatic colorectal cancer. *N Engl J Med*. 2004;351:337–345.
- Giltman JM, Ryden L, Cregger M, Bendahl PO, Jirstrom K, Rimm DL. Quantitative measurement of epidermal growth factor receptor is a negative predictive factor for tamoxifen response in hormone receptor positive premenopausal breast cancer. *J Clin Oncol*. 2007;25:3007–3014.
- Bellone S, Frera G, Landolfi G, et al. Overexpression of epidermal growth factor type-1 receptor (EGF-R1) in cervical cancer: implications for cetuximab-mediated therapy in recurrent/metastatic disease. *Gynecol Oncol*. 2007;106:513–520.
- Bonner JA, Harari PM, Giralt J, et al. Radiotherapy plus cetuximab for squamous-cell carcinoma of the head and neck. *N Engl J Med*. 2006;354:567–578.
- Addeo R, Caraglia M, Cerbone D, et al. Panitumumab: a new frontier of target therapy for the treatment of metastatic colorectal cancer. *Expert Rev Anticancer Ther*. 2010;10:499–505.
- Ramos TC, Figueredo J, Catala M, et al. Treatment of high-grade glioma patients with the humanized anti-epidermal growth factor receptor (EGFR) antibody h-R3: report from a phase I/II trial. *Cancer Biol Ther*. 2006;5:375–379.
- Crombet T, Osorio M, Cruz T, et al. Use of the humanized anti-epidermal growth factor receptor monoclonal antibody h-R3 in combination with radiotherapy in the treatment of locally advanced head and neck cancer patients. *J Clin Oncol*. 2004;22:1646–1654.
- Molinari E, De Quatrebarbes J, Andre T, Aractingi S. Cetuximab-induced acne. *Dermatology*. 2005;211:330–333.
- Keating GM. Panitumumab: a review of its use in metastatic colorectal cancer. *Drugs*. 2010;70:1059–1078.
- Lacouture ME. Mechanisms of cutaneous toxicities to EGFR inhibitors. *Nat Rev Cancer*. 2006;6:803–812.
- Rojo F, Gracias E, Villena N, et al. Pharmacodynamic trial of nimotuzumab in unresectable squamous cell carcinoma of the head and neck: a SENDO Foundation study. *Clin Cancer Res*. 2010;16:2474–2482.
- Garrido G, Tikhomirov IA, Rabasa A, et al. Bivalent binding by intermediate affinity of nimotuzumab: a contribution to explain antibody clinical profile. *Cancer Biol Ther*. 2011;11:373–382.
- De Roock W, De Vriendt V, Normanno N, Ciardiello F, Tejpar S. KRAS, BRAF, PIK3CA, and PTEN mutations: implications for targeted therapies in metastatic colorectal cancer. *Lancet Oncol*. 2011;12:594–603.
- De Roock W, Jonker DJ, Di Nicolantonio F, et al. Association of KRAS p.G13D mutation with outcome in patients with chemotherapy-refractory metastatic colorectal cancer treated with cetuximab. *JAMA*. 2010;304:1812–1820.
- Ojima F. Guided molecular missiles for tumor-targeting chemotherapy: case studies using the second-generation taxoids as warheads. *Acc Chem Res*. 2008;41:108–119.
- Hamblett KJ, Kozlosky CJ, Siu S, et al. AMG 595, an anti-EGFRVIII antibody-drug conjugate, induces potent antitumor activity against EGFRvIII-expressing glioblastoma. *Mol Cancer Ther*. 2015;14:1614–1624.
- LoRusso PM, Weiss D, Guardino E, Girish S, Sliwkowski MX. Trastuzumab emtansine: a unique antibody-drug conjugate in development for human epidermal growth factor receptor 2-positive cancer. *Clin Cancer Res*. 2011;17:6437–6447.
- Verma S, Miles D, Gianni L, et al. Trastuzumab emtansine for HER2-positive advanced breast cancer. *N Engl J Med*. 2012;367:1783–1791.
- Barok M, Joensuu H, Isola J. Trastuzumab emtansine: mechanisms of action and drug resistance. *Breast Cancer Res*. 2014;16:209–220.
- Shefet-Carasso L, Benhar I. Antibody-targeted drugs and drug resistance-challenges and solutions. *Drug Resist Updat*. 2015;18:36–46.
- Kovtun YV, Audette CA, Mayo MF, et al. Antibody-maytansinoid conjugates designed to bypass multidrug resistance. *Cancer Res*. 2010;70:2528–2537.
- Zhao RY, Wilhelm SD, Audette C, et al. Synthesis and evaluation of hydrophilic linkers for antibody-maytansinoid conjugates. *J Med Chem*. 2011;54:3606–3623.
- Chen Y. Drug-to-antibody ratio (DAR) by UV/Vis spectroscopy. *Methods Mol Biol*. 2013;1045:267–273.
- Fasih A, Fonge H, Cai Z, et al. <sup>111</sup>In-Bn-DTPA-nimotuzumab with/without modification with nuclear translocation sequence (NLS) peptides: an Auger electron-emitting radioimmunotherapeutic agent for EGFR-positive and trastuzumab (Herceptin)-resistant breast cancer. *Breast Cancer Res Treat*. 2012;135:189–200.
- Lindmo T, Bunn PA Jr. Determination of the true immunoreactive fraction of monoclonal antibodies after radiolabeling. *Methods Enzymol*. 1986;121:678–691.
- Ritter CA, Perez-Torres M, Rinehart C, et al. Human breast cancer cells selected for resistance to trastuzumab in vivo overexpress epidermal growth factor receptor and ErbB ligands and remain dependent on the ErbB receptor network. *Clin Cancer Res*. 2007;13:4909–4919.
- Erickson HK, Park PU, Widdison WC, et al. Antibody-maytansinoid conjugates are activated in targeted cancer cells by lysosomal degradation and linker-dependent intracellular processing. *Cancer Res*. 2006;66:4426–4433.
- Sorkin A, Dux JE. Quantitative analysis of endocytosis and turnover of epidermal growth factor (EGF) and EGF receptor. *Curr Protoc Cell Biol*. 2010;Chapter 15:Unit 15 14.
- Xu S. Internalization, trafficking, intracellular processing and actions of antibody-drug conjugates. *Pharm Res*. 2015;32:3577–3583.
- Smith LM, Nesterova A, Alley SC, Torgov MY, Carter PJ. Potent cytotoxicity of an auristatin-containing antibody-drug conjugate targeting melanoma cells expressing melanotransferrin/p97. *Mol Cancer Ther*. 2006;5:1474–1482.
- Law CL, Cerveny CG, Gordon KA, et al. Efficient elimination of B-lineage lymphomas by anti-CD20-auristatin conjugates. *Clin Cancer Res*. 2004;10:7842–7851.
- Berger C, Madhus IH, Stang E. Cetuximab in combination with anti-human IgG antibodies efficiently down-regulates the EGF receptor by macropinocytosis. *Exp Cell Res*. 2012;318:2578–2591.
- Veronese FM, Mero A. The impact of PEGylation on biological therapies. *Bio-Drugs*. 2008;22:315–329.
- Strop P, Delaria K, Foletti D, et al. Site-specific conjugation improves therapeutic index of antibody drug conjugates with high drug loading. *Nat Biotechnol*. 2015;33:694–696.
- Xie H, Audette C, Hoffee M, Lambert JM, Blattler WA. Pharmacokinetics and biodistribution of the antitumor immunoconjugate, cantuzumab mertansine (huC242-DM1), and its two components in mice. *J Pharmacol Exp Ther*. 2004;308:1073–1082.
- Hartimath SV, El-Sayed A, Makhlof A, et al. Therapeutic potential of nimotuzumab PEGylated-maytansine antibody drug conjugates against EGFR positive xenograft. *Oncotarget*. 2019;10:1031–1044.